The effects of austenite phase deformation on microstructure and magnetic properties in Fe–13.4%Mn–5.2%Mo alloy

T. Kırındı · U. Sarı

Abstract The effects of austenite phase deformation on martensitic transformations and magnetic properties in Fe–13.4%Mn–5.2%Mo have been investigated by scanning electron microscopy, transmission electron microscopy, and Mössbauer Spectroscopy. The increase of plastic deformation rates on austenite phase created considerable changes in amounts of ε (h.c.p.) and α'(b.c.c.) martensite, and austenite grains size decreased. Analysis of microstructure and Mössbauer spectra show that the amount of ε martensite increased at low deformation rates whereas it decreased at high deformation rate. Besides, Mössbauer spectra of the alloy reveal a ferromagnetic character with a broad sextet for α' martensite phase and a paramagnetic character with a singlet for the γ (f.c.c.) austenite and ε martensite phases. In the other hand, the magnetic character of the alloy exhibits a different magnetic order depending on strain rates.

Introduction

It has been reported in previous studies that two distinct types of martensitic transformation with deformation or thermal effects in Fe–Mn based alloys, namely ε and α' martensites, might occur depending on the Mn content in the austenite γ phase [1–4]. Owing to the influence of various physical factors, thermal treat and plastic deformations are a lot complicated, especially in austenite polycrystalline alloys where local stress might be complex. Several studies indicated that pre-strain and martensite phase deformations influenced martensitic transformation in Fe–Mn based alloys [5–9]. The deformation of these alloys causes stress-induced ε martensite and the formation made of stress-induced martensite describes how martensite formation occurs. The crystal defects formed by deformation and thermal treat play an important role on the mechanism of martensitic transformation [10–15]. Besides, deformation rate causes crystal defects in matrix phase and thus, stress-induced ε martesite can easily be formed. Also stacking faults (SF) play an important role on formation of the stress-induced ε martensite.

In the Fe–Mn based alloys, there is a strong relationship between the magnetic behavior and austenite–martensite phase transformation. In spite of paramagnetic nature of austenite phase, the martensite product phase may exhibit ferromagnetic, antiferromagnetic, and paramagnetic behaviors on different conditions [16–18]. A paramagnetic → antiferromagnetic order reaction can also occur upon cooling in both austenite and martensite phases of Fe–Mn alloys, and such a magnetic transition in austenite phase stabilizes γ phase relatively to the competing ε phase [3]. Kırındı and Sarı [1] studied in detail the magnetic properties and thermal-induced martensitic transformation in Fe–Mn–Mo alloys. The aim of this study is to examine and clarify the characteristics of deformation induced martensites in Fe–13.4%Mn–5.2%Mo alloy according to existing martensite morphology, crystallography, and magnetism by scanning electron microscopy (SEM), transmission electron microscopy (TEM), and Mössbauer Spectroscopy.

T. Kırındı (✉)
Department of Computer Education and Instructional Technology, Kırıkkale University, Yahsihan Campus, 71450 Kırıkkale, Turkey
e-mail: talipkirindi@yahoo.com

U. Sarı
Department of Elementary Education, Elementary Science Education, Kırıkkale University, Yahsihan Campus, 71450 Kırıkkale, Turkey

Table 1 Heat treatment and compressed deformations

Samples	Natural of heat treatment and compressed deformation
A_0	Homogenized at 1200 °C for 12 h and cooled in furnace
A_1	Homogenized at 1200 °C for 12 h and cooled in water bath at room temperature
B	Compressed by 6% deformation at room temperature of samples A_0 and homogenized at 1000 °C for 30 min then cooled in water bath at room temperature
C	Compressed by 10% deformation at room temperature of Samples A_0 and homogenized at 1000 °C for 30 min then cooled in water bath at room temperature
D	Compressed by 20% deformation at room temperature of Samples A_0 and homogenized at 1000 °C for 30 min then cooled in water bath at room temperature

Experiments

The alloy used in this study was prepared by vacuum induction melting under an argon atmosphere from pure (99.9%) alloying elements and quenching as cylindrical rods with 1 cm diameter and 10 cm length. The chemical composition of the alloy was obtained as Fe–13.4%Mn–5.2%Mo (wt.%) by using electron dispersion spectroscopy technique.

The arc-melted ingots were cut by a diamond saw at room temperature. Compression specimens were made in the shape of rectangular blocks 9 mm in length and with cross sections 5×5 mm^2. The heat treatment and plastic deformation rates of sealed specimens were given in Table 1. The specimens were compressed at a strain rate of 350 μm/min at room temperature. For SEM observations,

the surface of the sample was first mechanically polished and afterward the damaged surface layer was eliminated by etching in a solution composed of 5% nitric acid and 95% methanol for 30 s. SEM observations were made in a JEOL 5600 scanning microscope operated at 20 kV.

Thin foils were prepared for TEM using double-jet electro-polishing in Streurs-Tenupol jet unit with a solution of 92% acetic acid and 8% perchloric acid at 10 °C and a voltage of 20 V. The TEM observations were performed by a JEOL 3010 electron microscope operated at 300 kV with a double tilt specimen.

Mössbauer spectroscopy was applied to study the magnetism and volume fractions of both the austenite and martensite phases. Specimens examined by SEM were used for Mössbauer spectroscopy measurements at room temperature. A spectrometer with a 50 mCi ^{57}Co radioactive source (diffused in Rh) was used during study. A Normos-90 computer program was used to find out the Mössbauer parameters and relative volume fractions of the austenite and martensite phases. The Mössbauer spectra of examined sample were calibrated with respect to α-Fe, and isomer shifts were given relative to the center of the α-Fe.

Results and discussion

To get information about the microstructural characteristics of Fe–13.4%Mn–5.2%Mo alloy, we carried out SEM and TEM observations. Figure 1 shows the secondary electron image SEM micrograph of the microstructure forming in the samples. The austenite grains and two types of

Fig. 1 SEM micrographs of samples: **a** sample A_1, **b** sample B, **c** sample C, **d** sample D

J Mater Sci (2011) 46:6378–6383
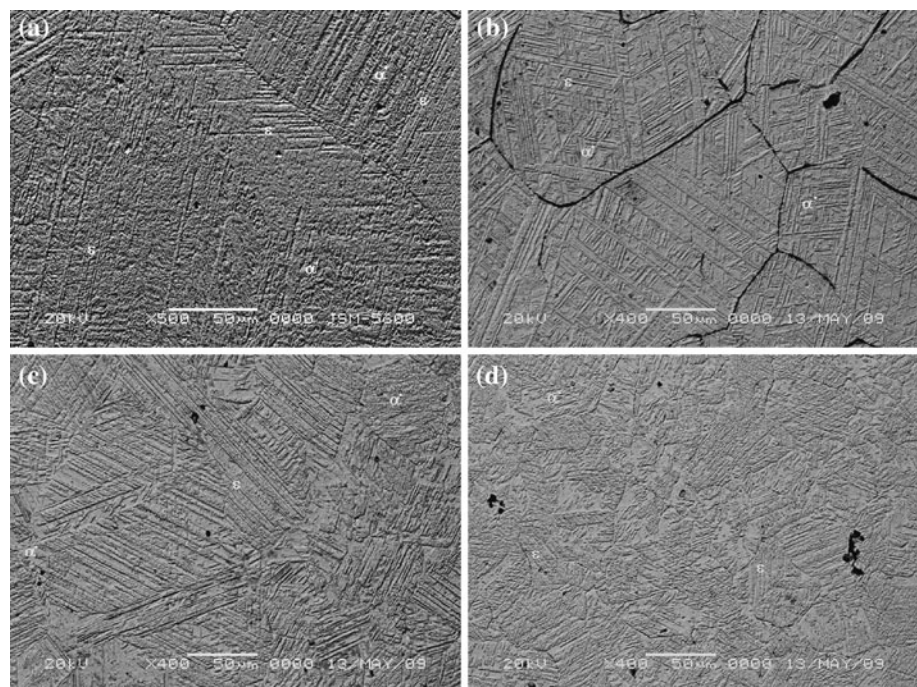
martensite crystals which have different morphologies in the grains appear clearly in this figure. Figure 1 shows that the sizes of austenite grains decrease with increasing amount of plastic deformation. More crystal defects formed by plastic deformation of austenite phase may cause decreasing of the grain size. As a result, the total grain boundary area is relatively increased when the austenite grains are smaller. This causes an increase in the number of possible nucleation sites, thus the formation of martensite becomes easier [2].

Figure 1a shows obviously that two types of thermal-induced martensites, ε and α' martensites, coexist in the alloy. While the ε martensite plates appear generally as parallel stacks of fine bands, the α' martensites form as little particles in thin plates tangle. In addition, Fig. 1 reveals that thermal and deformation induced martensites clearly appeared with different morphology. Figure 1b, c show the microstructure of austenite phase deformed on 6 and 10% rates (samples B and C). When Fig. 1a, b, c are compared, it can be seen that the amount of ε plates increased in the case of deformation. More ε martensite is induced when the low compression stress are applied to the alloy in austenite state, because the deformation provides more nuclei for stress-induced ε martensite [4, 12, 19]. Figure 1d shows α' crystal particles occurred in austenite grains and intersection of ε martensite plates. With 20% plastic deformation of austenite phase, the amount of ε phase decreases while α' martensite phase increases. This result indicates that 20% plastic deformation can cause to $\gamma \rightarrow \alpha'$ or $\gamma \rightarrow \varepsilon \rightarrow \alpha'$ transformation. The studies on the austenite–martensite phase transformations in Fe–Mn alloys have revealed that austenite (γ) phase can transform to α' and ε martensites, and $\varepsilon \rightarrow \alpha'$ transformation is also possible under some physical conditions [12, 13, 20]. The $\gamma \rightarrow \varepsilon \rightarrow \alpha'$ transformation can be induced by deformation. It is inferred from this fact that the α' crystal in this study may not be transformed directly from the austenite but may be formed from the ε phase. $\gamma \rightarrow \alpha'$ and $\gamma \rightarrow \varepsilon \rightarrow \alpha'$ transformations can easily be distinguished from one another by thermal dilatometer technique despite the fact that there is no appreciable difference in their transformation temperatures. Besides, α' martensite crystals formed by ε phase transformation are extremely small compared to the α' martensite formed directly from the austenite γ phase [4].

Figure 2 shows the TEM bright field image of austenite phase in sample A_0. Here the SF, discrete dislocations, grain boundary (GB), and network of dislocations appear obviously in austenite phase. The SF plays an important role in the formation of ε martensite because they create embryos for the ε martensite formation. The models describing ε martensite formation are based on the assumption of over-lapping SF on every second

close-packed plane of the austenite phase and the transformation occurs with the movement $a_\lambda/6\langle112\rangle$ Shockley partial dislocations. Therefore, ε martensite formation is primarily observed in the alloys with low stacking fault energies [12, 13]. Figure 3 shows the TEM bright field image and selected area electron diffraction patterns of Sample C at room temperature. The ε and α' martensite plates are clearly seen in Fig. 3a. The diffraction patterns taken from ε and α' martensite plates are given in Fig. 3b and c, respectively. The zone axis for ε and α' martensite phases determined as $[221]_\varepsilon$ and $[100]_{\alpha'}$ obtained from the analysis of diffraction pattern. In general, ε martensite plates formed parallel arrays which exhibit relatively large bands structure (Fig. 3a). The existence of dislocation creates two competing effects in austenite structure, namely, stimulation of martensite structures due to the formation of favorable nucleation sites and inhibition of growth by the faulted austenite substructure. The latter effect is generally dominant during austenite $\rightarrow \varepsilon$ martensite transformations in Fe–Mn based alloys and the ε martensite formation is suppressed with increasing amount of plastic deformation. The formation of the α' martensite crystals has been established to be mainly associated with dislocations in prior austenite phase and they appear on
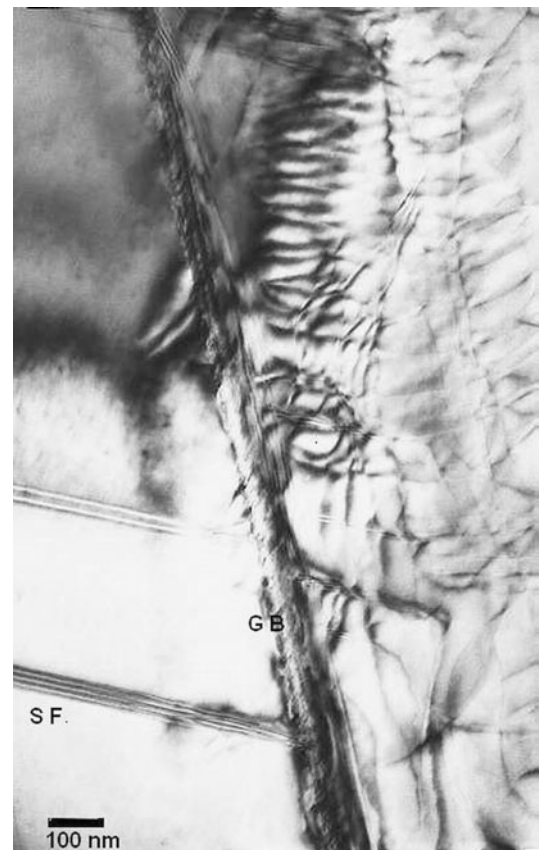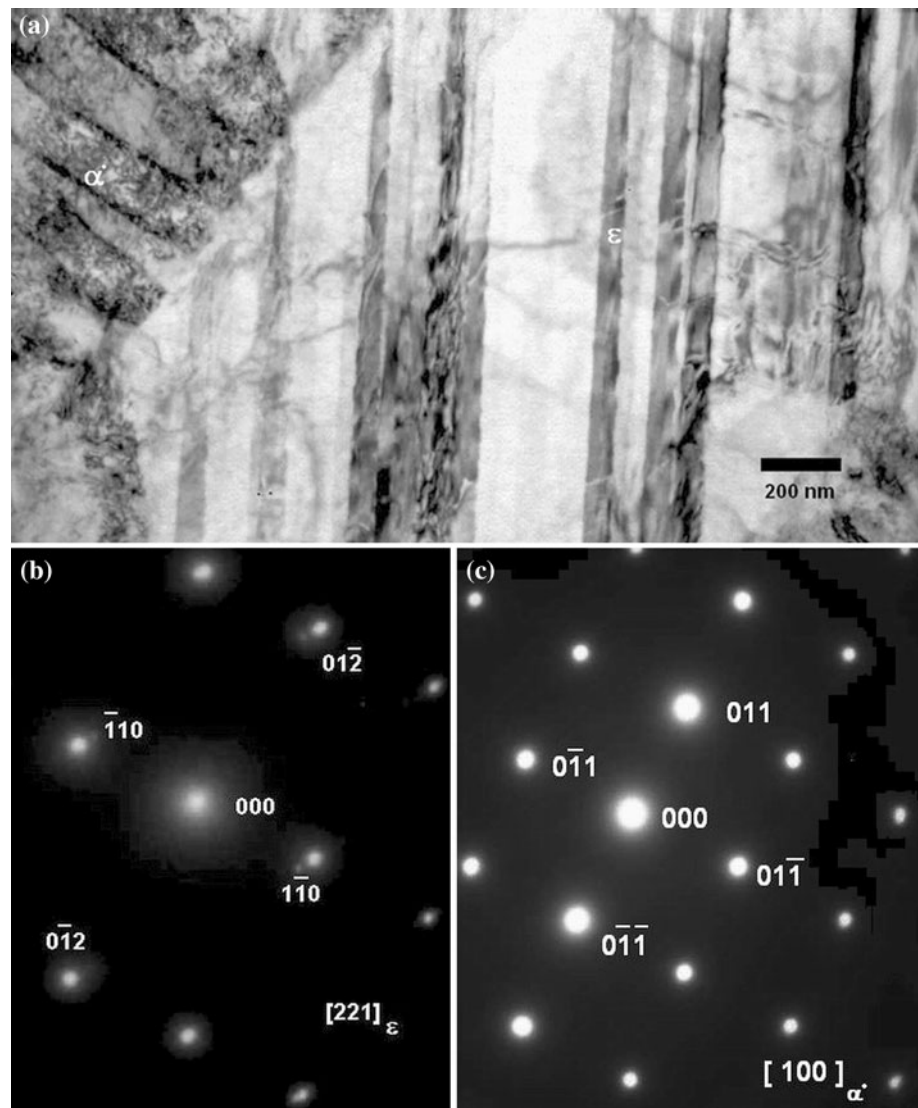

Fig. 2 TEM micrograph of furnace cooled specimen (A_0)

Springer

Fig. 3 TEM images and selected area diffraction patterns of sample C: **a** bright field electron micrograph, **b** electron diffraction pattern of the ε martensite plate, and **c** electron diffraction pattern of the α' martensite plate

dislocated austenite areas [2]. In Fig. 4, the microstructure of Sample D shows the α' and ε martensite and network of dislocation in the austenite phase. The effect of high plastic deformation rates of austenite phase caused formation of less ε martensite, while it formed precious α' crystals as seen in this Figure. It seen that the networks of dislocation occurred in austenite phase played important roles on the size of austenite grains and formation of martensite phases.

The magnetic characters of the austenite and martensite phases have been examined with Mössbauer spectroscopy technique. Figure 5 shows the Mössbauer spectra obtained from deformation and undeformation samples at room temperature (Table 1). The spectra are characterized by a broad sextet and a central singlet in the alloy. In Mössbauer spectroscopy, ferromagnetic (or antiferromagnetic) character of materials displays a typical sextet whereas paramagnetic structure exhibits only a singlet. Furthermore, it is known that α' (b.c.c.) phase is ferromagnetic while γ

(f.c.c.) and ε (h.c.p.) phases display generally paramagnetic character in Fe–Mn alloys [16–18]. Therefore, in Fig. 5, the sextet belongs to ferromagnetic α' martensite phase as the paramagnetic singlet can be ascribed either to γ austenite phase or to ε martensite phase. These results show that the paramagnetic $\rightarrow$ ferromagnetic transition occur also along with $\gamma \rightarrow \alpha'$ or $\gamma \rightarrow \varepsilon \rightarrow \alpha'$ martensitic transformation in the alloy. This Figure exhibits that ferromagnetic sextet area and paramagnetic singlet area clearly changed under the different plastic deformation rates. It stems from the change of martensite structure depending on deformation rate.

In addition to the $\gamma \rightarrow \varepsilon$ and $\gamma \rightarrow \alpha'$ martensite transformations, a magnetic transition from paramagnetism to antiferromagnetism can occur at Neel temperatures (T_N) on cooling in γ and ε phases of these alloys. These magnetic transitions appear as split doublet in Mösbauer spectra [21–24]. Nevertheless, such a doublet does not emerge in

Fig. 4 TEM micrograph of sample D

Fig. 5 Mössbauer spectra of samples at room temperature

Fig. 5, and it displays that the paramagnetic → antiferromagnetic transitions does not occur in quenched alloy at room temperature. According to the results found in literature [16–18, 22], Neel temperatures of both paramagnetic γ and ε phases in the Fe–Mn alloys which is below 15 wt%Mn content are lower than room temperature and M_s. In the other words, martensitic transformations in these alloys occur above T_N, and therefore, there is no effect of the magnetic transition in the martensitic transformations. In this case, it can be said that T_N of the alloy is also below room temperature according to the Mössbauer spectra (Fig. 5). Consequently, γ and ε phases of the Fe–13.4%Mn–5.2%Mo alloy have paramagnetic characters, and the central singlet in Fig. 5 belongs to both paramagnetic γ and ε phases. It is almost impossible to sort these phases out by Mössbauer spectrometry at room temperature [24]. The Mössbauer parameters such as isomer shifts (δ), hyperfine magnetic fields (B_{hf}) with the calculated % volume fractions of phases are given in Table 2. Here, the volume fractions of ε and γ phases is evaluated together owing to the fact that ε and γ phases can not be distinguished from each other by Mössbauer spectrometry at room temperature. As it is seen in the Table 2, deformation rates clearly affected the
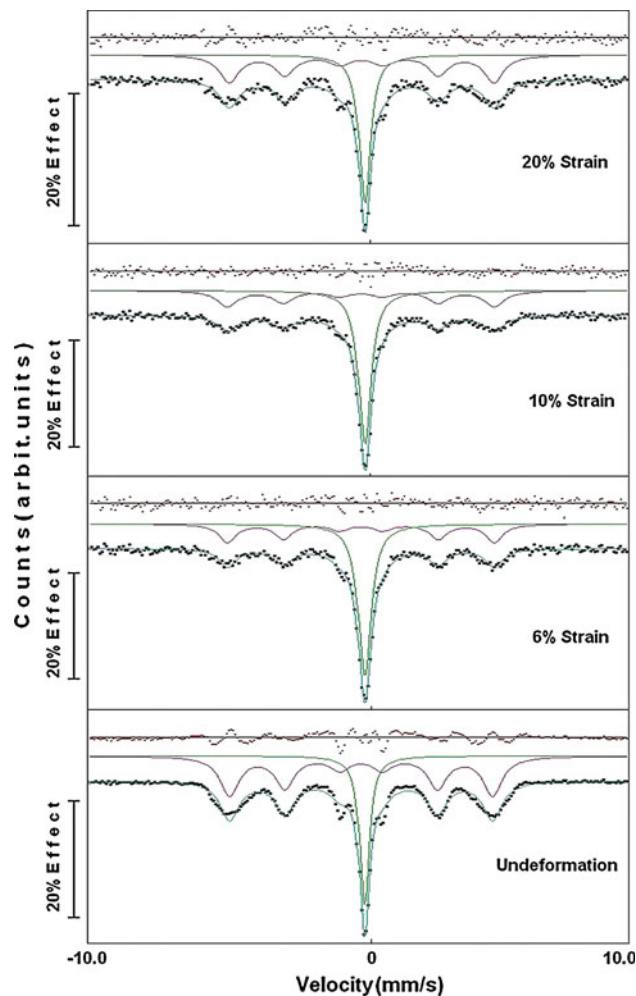
magnetic ordering and % volume transformation fraction of phases in the alloy. The amount of α' martensite is much higher than the ε martensite in samples A_1 and D. On the other hand, the amount of α' martensite decreased in sample B and C (6 and 10% deformation rates). These results confirm with present SEM and TEM observation and it means that the shape memory effect of alloy can be developed with low deformation rate of austenite phase. The internal magnetic field value of α' martensite phases in sample A_1–D is given in Table 2.

Conclusions

The effects of austenite phase deformation on martensitic transformations in Fe–13.4wt% Mn–5.2wt% Mo alloy were investigated by using SEM and TEM. ε and α' martensite structures determined in this alloy by the electron diffraction patterns analysis. The deformation on austenite phase significantly affects the type and amount of

Table 2 Some Mössbauer parameters of the alloy

Sample	$\gamma + \varepsilon$ phase (%)	α' phase(%)	$\delta_{\gamma+\varepsilon} \pm 0.002$ (mm/s)	$\delta_{\alpha'} \pm 0.001$ (mm/s)	B_{hf} (α') (Tesla)
A_1	28.13	71.86	−0.237	−0.1104	30.54
B	46.02	54	−0.241	−0.107	30.52
C	58.60	41.40	−0.237	−0.103	30.78
D	42.50	57.50	−0.241	−0.125	30.5

martensite. While ε martensite amount is lower than α' martensite amount within high deformation rates, α' martensite amount is lower than ε martensite amount within low deformation rate. Thus, the shape memory effect of alloy can be developed with low deformation rate of austenite phase. The SEM observation show that increasing deformation rates reduced austenite grains size, in other words, growing of austenite grains size is obstructed by the crystal defects formed by plastic deformation.

The Mössbauer spectra of the alloy clearly show that the α' martensite phase has a ferromagnetic character whereas the γ austenite and ε martensite phases display a paramagnetic character. The spectra revealed that paramagnetic $\rightarrow$ ferromagnetic transition occurs along with $\gamma \rightarrow \alpha'$ or $\gamma \rightarrow \varepsilon \rightarrow \alpha'$ martensite transformation in the alloy. Consequently, ferromagnetic ordered was changed with increasing plastic deformation rates in this alloy.

References

1. Kırındı T, Sarı U (2009) J Alloys Compds 488:129
2. Durlu TN (1997) J Mater Sci Lett 16:320
3. Sarı U, Kırındı T, Yüksel M, Ağan S (2009) J Alloys Compds 476:160
4. Nishiyama Z (1978) Martensitic transformation. Academic Press, London
5. Durlu TN (1999) J Mater Sci 34:2887. doi:10.1023/A:1004691503634
6. Kırındı T, Sarı U, Dikici M (2009) J Alloys Compds 475:145
7. Kirindi T, Dikici M (2006) J Alloys Compds 407:157
8. Dong ZZ, Kajiwara S, Kikuchi T, Sawaguchi T (2005) Acta Mater 53:4009
9. Dergeon N, Kajiwara S, Kikuchi T (2000) Acta Mater 48:4053
10. Jun J-H, Kong D-K, Choi C-S (1998) Mater Res Bul 33:1419
11. Sarı U, Güler E, Kırındı T, Dikici M (2009) J Phys Chem Solids 70:1226
12. Bergeon N, Guenin G, Esnouf C (1998) Mater Sci Eng A242:77
13. Bergeon N, Guenin G, Esnouf C (1998) Mater Sci Eng A242:87
14. Sawaguchi T, Bujoreanu L-G, Kikuchi T, Ogawa K, Koyama M, Murakami M (2008) Scr Mater 59:826
15. Baruj A, Troiani HE (2008) Mater Sci Eng A 481–482:574
16. Mizrahi M, Cabrera AF, Cotes SM, Stewart SJ, Mercader RC, Desimoni J (2004) Hyperfine Interact 156/157:541
17. Cotes SM, Cabrera AF, Damonte LC, Mercader RC, Desimoni J (2002) Hyperfine Interact 141/142:409
18. Martinez J, Aurelio G, Cuello G, Cotes SM, Guillermet AF, Desimoni J (2005) Hyperfine Interact 161:221
19. Durlu TN (1995) J Mater Sci Lett 14:1604
20. Kirindi T, Güler E, Dikici M (2007) J Alloys Compds 433:202
21. Acet M, Schneider T, Gehrmann B, Wassermann EF (1995) J Phys IV 5:379
22. Marinelli P, Baruj A, Cotes S, Guillermet AF, Sade M (1999) Mater Sci Eng A 273–275:498
23. Martinez J, Cotes SM, Cabrera AF, Desimoni J, Guillermet AF (2005) Mater Sci Eng A 408:26
24. Cotes SM, Cabrera AF, Damonte LC, Mercader RC, Desimoni J (2002) Physica B 320:274